Magneto-electrostatic trapping of ground state OH molecules

Brian C. Sawyer,* Benjamin L. Lev, Eric R. Hudson,† Benjamin K. Stuhl, Manuel Lara, John L. Bohn, and Jun Ye
JILA, National Institute of Standards and Technology and the University of Colorado
Department of Physics, University of Colorado, Boulder, Colorado 80309-0440, USA
(Dated: February 2, 2008)

We report the magnetic confinement of neutral, ground state hydroxyl radicals (OH) at a density of $\sim 3\times10^3$ cm^{-3} and temperature of $\sim$30 mK. An adjustable electric field of sufficient magnitude to polarize the OH is superimposed on the trap in either a quadrupole or homogenous field geometry. The OH is confined by an overall potential established via molecular state mixing induced by the combined electric and magnetic fields acting on the molecule's electric dipole and magnetic dipole moments, respectively. An effective molecular Hamiltonian including Stark and Zeeman terms has been constructed to describe single molecule dynamics inside the trap. Monte Carlo simulation using this Hamiltonian accurately models the observed trap dynamics in various trap configurations. Confinement of cold polar molecules in a magnetic trap, leaving large, adjustable electric fields for control, is an important step towards the study of low energy dipole-dipole collisions.

PACS numbers: 33.80.Ps, 33.55.Be, 39.10.+j, 33.15.Kr

Cold and ultracold molecules are currently subject to intense research efforts as they promise to lead major advances in precision measurement, quantum control, and cold chemistry [1]. Much of this interest has focused on molecules possessing permanent electric dipole moments. The long range, anisotropic dipole-dipole interaction leads to novel collision [2, 3] and reaction [4] dynamics, and may serve as the interaction between molecular qubits [5] in architectures for quantum information processing [6]. Quantum phase transitions can be explored with polar molecules [7]. Furthermore, polar molecules may possess extremely large internal electric fields (on the order of GV/cm), yielding dramatic sensitivity enhancement to searches for an electron electric dipole moment [8, 9]. Cold polar molecules have been produced via photoassociation of ultracold atomic species [10, 11], Stark deceleration [12, 13], and buffer gas cooling [14].

Polar molecules are readily trapped in inhomogeneous electric fields [15, 16], however theory suggests that at high phase-space densities such traps invariably suffer from large inelastic collision losses [17]. One possible solution is to trap strong-field seeking states via time-dependent electric traps [18]. In contrast, we are interested in magnetically trapping these neutral polar molecules so as to have the freedom to apply external electric fields to control collision dynamics inside the trap. Highly vibrationally excited, triplet KRb molecules produced via photoassociation have been magnetically trapped at a temperature of $\sim$300 μK and density of 10^4 cm^{-3} [19]. Buffer gas cooling has been used to load a magnetic trap with ground-state CaH and NH molecules at temperatures of hundreds of mK and densities of $\sim 10^8$ cm^{-3}, but in the presence of a cold He buffer gas [14, 20]. We report here the first observation of magnetically trapped hydroxyl radical (OH) molecules and the lowest temperature (30 mK) yet achieved for a magnetically-trapped polar molecule in its rovibronic ground state. Moreover, we perform the first study of trap dynamics based on a single molecule possessing large magnetic and electric dipole moments in B- and E-fields that are inhomogeneous and anisotropic. Interesting polar molecule dynamics have been predicted at large field strengths [21]. Accurate correspondence between experimental data and simulations is achieved only by accounting for the molecular state mixing induced by the crossed fields. Large magnetic (B) fields may serve to suppress inelastic collision losses [22] while at the same time sympathetic cooling of molecules via co-trapped ultracold atoms may become feasible [23]. In addition, the magnetic quadrupole trap described here permits the application of arbitrary external electric (E) fields to a large class of polar molecules—a necessary step towards observing cold molecule dipole-dipole collisions [24].

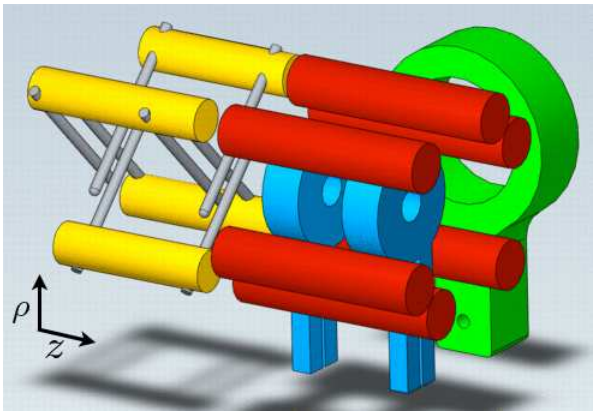

FIG. 1: (color online) Illustration of the magneto-electrostatic trap (MET) assembly. The terminus of the Stark decelerator (yellow, gray electrodes), shown to the left, couples state-selected cold molecules into the magnetic quadrupole (blue). The double-electrode structures within the electric quadrupole (red) allow for application of uniform electric fields within the magnetic trap. The ring (green) supports a 1 inch lens for collection of laser-induced fluorescence.

To magnetically trap OH, we begin with a cold beam of ground state ($^2\Pi_{3/2}$) OH produced via a pulsed electric discharge through 2% H_2O vapor [25] seeded in 1.5 bar of Kr. A piezoelectric transducer valve [26] operating at 10 Hz provides a supersonic expansion of the OH/Kr mixture through a 1 mm nozzle. This results in a 490 m/s molecular packet with a 15% longitudinal ($\hat{z}$) velocity spread. The transverse ($\hat{\rho}$) velocity spread of the beam is limited to 2% by the 3 mm diameter molecular skimmer. Compared with a Xe expansion, the higher-velocity Kr expansion leads to less transverse beam loss within the current decelerator design. Thus, despite the fact that the Kr beam requires a higher phase angle for deceleration (smaller decelerator acceptance) it results in more decelerated molecules. After passing through the skimmer, the OH packet is spatially matched to the decelerator entrance via an electrostatic hexapole. Details regarding the OH Stark decelerator design and operating principle may be found in previous work [27, 28]. We utilize the 142 stages of our Stark decelerator to slow a 130 mK packet (in the co-moving frame) of OH to 20 m/s at a phase angle $\phi_0 = 47.45°$ for coupling into the magneto-electrostatic trap (MET). Decelerated OH packets are detected via laser-induced fluorescence (LIF) upon entering the MET, whose center lies 2.7 cm from the final pair of decelerator rods. The 282 nm pulsed laser beam is oriented along the mutual longitudinal axis ($\hat{z}$) of the decelerator and MET, and the resulting 313 nm LIF is collected in a solid angle of 0.016 sr.

The MET is illustrated in Fig. 1, and consists of two copper coils operated in an anti-Helmholtz configuration surrounded by an electric quadrupole. The center-to-center magnetic coil spacing is 1.5 cm, providing a field gradient of 6700 G/cm by passing 1500 A through the 4 turns of each water-cooled coil. A longitudinal trap depth of 400 mK is achieved, while the electrodes surrounding the coils allow the application of an E-field to the trapped sample. The double- and single-rod electrodes that comprise the electric quadrupole allow the application of two distinct field configurations. A uniform bias electric field is created by grounding the single-rods while oppositely charging the opposing double-rods to ±3 kV. Alternatively, we generate a quadrupole E-field by charging neighboring rods with opposite polarities of ±9 kV. Shielding by the MET coils reduces the interior E-field by a factor of ∼5. Figure 2 depicts the quadrupole electric field superimposed on the magnetic quadrupole field. OH has both an appreciable magnetic and electric dipole, and we can easily alter the geometry of the trapping potential by applying electric fields of variable magnitude and direction to the magnetically trapped sample.

The OH ground state is best described by Hund's case (a), in which the spin ($|\Sigma| = \frac{1}{2}$) and orbital ($|\Lambda| = 1$) angular momenta are strongly coupled to the molecular axis, yielding the total angular momentum projection $|\Omega| = \frac{3}{2}$. The $|\Omega| = \frac{1}{2}$ state lies 126 cm^{-1} above this

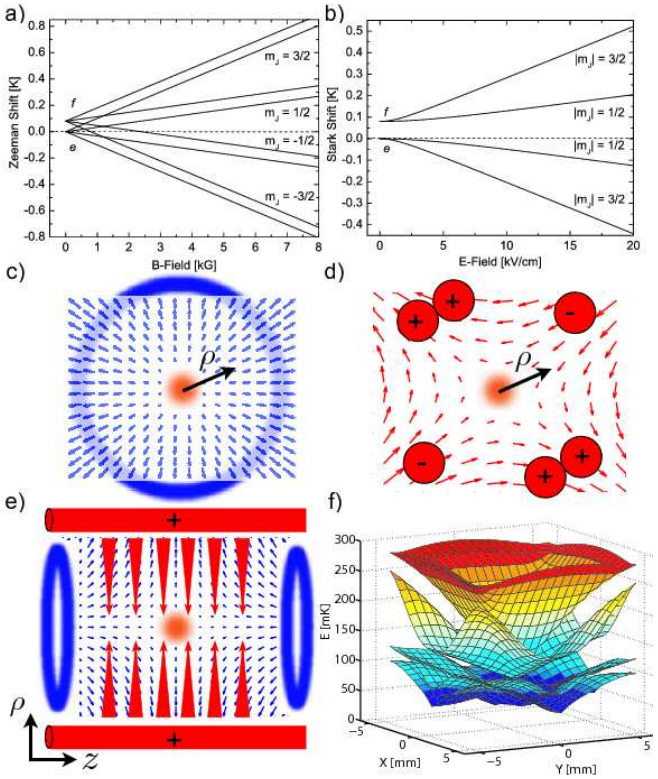

FIG. 2: (color online) (a) Zeeman and (b) Stark effects of the ground state structure of OH. (c) Magnetic and (d) electric quadruple fields viewed from $\hat{z}$. (e) Side view of the MET configuration with quadrupole E and B fields. (f) Transverse adiabatic potential surfaces for various components of the OH ground state at the longitudinal MET center. The top surface depicts the decelerated/trapped $|J = \frac{3}{2}, m_J = \frac{3}{2}\rangle$ state.

ground state. The nuclear spin of the hydrogen atom ($I = \frac{1}{2}$) leads to a hyperfine splitting of the ground state into $F = 2, 1$ components. In the presence of large external fields (E>1 kV/cm or B>100 G), the electron angular momentum and nuclear spin decouple [5], and one considers the total angular momentum **J**, which includes nuclear and electronic orbital angular momentum as well as electron spin. The projections m_J of **J** are defined along the axis of the applied field. The ground state is further split into two opposite-parity states (f/e) by the coupling of electronic orbital angular momentum to nuclear rotation. This small Λ-doublet splitting of 1.67 GHz, along with the 1.67 D electric dipole, is responsible for the rather large Stark shift experienced by OH molecules [29]. Fig. 2(a) and (b) show the Zeeman and Stark effects of the OH ground-state respectively. External electric fields can thus dramatically alter the potential confining the magnetically trapped molecules. Fig. 2(c-e) illustrate the field geometries within the MET. In the plane perpendicular to $\hat{z}$, Fig. 2(c) shows the radial B-field characteristic of a magnetic quadrupole, while Fig. 2(d) depicts the electric quadrupole field introduced

by the electrode geometry. Fig. 2(e) illustrates both B (blue) and E (red) fields along $\hat{z}$.

The top potential surface of Fig. 2(f) represents the energy shift of the decelerated $|J=\frac{3}{2}, m_J=\frac{3}{2}\rangle$ state (E-fields couple e and f, therefore they are no longer good quantum numbers) within the combined quadrupole E- and B-fields present in the MET. The transverse profiles of the four trapping adiabatic potentials are depicted at the longitudinal trap center, where $\overrightarrow{B}\cdot\hat{z}=0$. The remaining four surfaces (not shown) are simply inverted relative to those displayed, and are therefore anti-trapping. The three-dimensional MET potentials are calculated by diagonalizing an effective Hamiltonian that includes both Stark and Zeeman terms. Coupling between the ground $|J=\frac{3}{2}, \Omega=\frac{3}{2}\rangle$, and excited $|\frac{5}{2},\frac{3}{2}\rangle$, $|\frac{1}{2},\frac{1}{2}\rangle$, $|\frac{3}{2},\frac{1}{2}\rangle$ states is included, for a total of 64 hyperfine components. The $|J=\frac{3}{2}, \Omega=\frac{3}{2}\rangle$, $|\frac{3}{2},\frac{1}{2}\rangle$ coupling is the most critical, increasing the trap depth of the top surface of Fig. 2(f) by 11%. Addition of the remaining states modifies the potential by <0.1%. The square shape of the top surface is a result of the varying angle between E and B in the MET. The potentials from each field directly sum where the fields are collinear, but the trap shallows from this maximum value as the angle between E and B increases.

The Stark decelerator slows only those OH molecules in the electrically weak-field seeking (EWFS) component of the ground state, *i.e.*, the upper Λ-doublet. Of these EWFS molecules, only those with components $J=\frac{3}{2}$, $m_J=\pm\frac{3}{2}$ are synchronously slowed to 20 m/s. Because the positive m_J state is magnetically weak-field seeking, only 50% of the decelerated molecular packet is trappable by the MET. The molecules experience a B-field >100 G at the last deceleration stage emanating from the back coil, preserving the quantization of the decelerated state.

To trap the incoming OH packet, the coil closer to the decelerator (front coil) is grounded while the coil further from the decelerator (back coil) operates at 2000 A for the duration of the 3.7 ms deceleration sequence. The effective magnetic dipole of OH in its $J=m_J=\frac{3}{2}$ state is 1.2 $\mu_B \simeq 0.81$ K/T, where μ_B is the Bohr magneton, allowing the back coil to stop molecules with velocity $\leq$ 22 m/s. The front coil is turned on after the 20 m/s molecules are stopped by the back coil, which occurs 2.65 ms after exiting the final deceleration stage. The trap switching is synchronous to the 20 m/s molecules since OH possessing larger longitudinal velocities escape the quadrupole field. For technical reasons, the two magnet coils are connected in series, causing the current in both coils to decrease from 2000 A to 1500 A over ∼800 μs once the front coil is switched into the circuit. This problem will be addressed with a current servo.

Figure 3 displays typical time-of-flight data resulting from the trapping sequence along with results from Monte Carlo simulation of the trap dynamics. The large initial peak is the decelerated OH packet traversing the detection region at the center of the trap. All subsequent

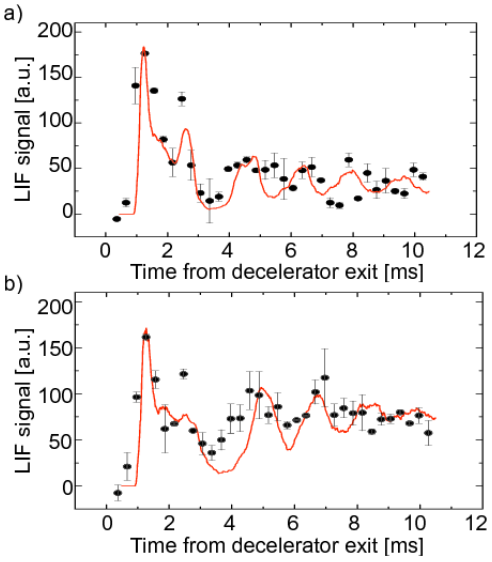

FIG. 3: (color online) Time-of-flight data and Monte Carlo simulation results (solid red line) for two different MET configurations. The magnetic field switches from the stopping configuration to quadrupole trapping at $t = 2.65$ ms. (a) Magnetic trap only. (b) Stopping and trapping in the presence of combined electric and magnetic quadrupole fields. Note larger steady-state trap population.

peaks are the result of oscillation in the $\hat{\rho}$ dimension, with a frequency of ∼650 Hz. Fluorescence is gathered in $\hat{\rho}$, and oscillations in $\hat{z}$ are not detectable since our detection region spans the entire visible trap length. The magnetic quadrupole trap is unable to confine all the molecules stopped by the back coil alone due to the 25% current drop, as is clear from the difference in signal height at ∼2.5 ms versus the steady-state level at, e.g., 10 ms. Note the larger steady-state population of Fig. 3(b) from the addition of a confining transverse electric quadrupole. Also visible is the shorter coherence time compared to Fig. 3(a), which results from trap distortion visible in Fig. 2(f). An estimate of the density of trapped OH, as measured by LIF, gives $\sim 3\times10^3$ cm^{-3}. By comparison, the density of a packet "bunched" at a phase angle of $\phi_0 = 0°$ is 10^7 cm^{-3}, while the 20 m/s packet is 10^4 cm^{-3}. Monte Carlo analysis of the velocity distribution of the trapped OH yields temperatures of ∼30 mK. With our improved knowledge of the trap dynamics due to accurate Monte Carlo simulations, we expect to be able to trap 2-3 times more OH through modification of deceleration phase angle and trap switching times for optimal coupling of the slowed beam into the MET.

Higher decelerator phase angles should, in principle, produce a slower OH packet. However, below 20 m/s the OH population drops sharply and no further deceleration is observed. We attribute this effect to a reduction in the effective aperture seen by slow molecules as they traverse the final deceleration stage. The OH closest to the final

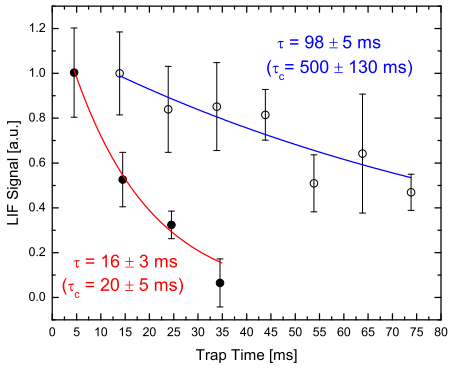

FIG. 4: (color online) Measured (τ) and de-convolved collisional (τ_c) lifetimes of magnetically trapped OH at a background pressure of 1×10^{-6} Torr (•, red line) and 4×10^{-8} Torr (○, blue line).

decelerator rods see a larger longitudinal potential than those on-axis, and at sufficient phase angles, are stopped or reflected and hence cannot be observed in the MET region. Numerical models elucidate this effect, which may be mitigated by new decelerator designs [30].

The 10 Hz repetition rate of our Stark decelerator currently limits our trap interrogation time to 100 ms. Maintaining continuous currents of 1500 A presents technical challenges due to heating in both the switching transistors and cabling. To mitigate this, we operate the switching MOSFETs on a water-cooled copper plate and also run chilled water through the MET coils. Water-cooled cables are also necessary for such high-power operation. Figure 4 shows electric field-free OH trap lifetimes measured in two different background pressure regimes: 1×10^{-6} and 4×10^{-8} Torr, both dominated by N_2 at 295 K. Non-ideal power supply control causes the trap current to decrease from 1500 A to 1160 A at a rate of 2000 A/s. This lowers the trap depth, resulting in a loss of 12 ± 2 s^{-1}. After accounting for this loss mechanism, we find background collision-limited lifetimes of 20 ± 5 ms and 500 ± 130 ms for the two pressure regimes, respectively. These lifetimes determine an OH-N_2 collision cross section of 500 ± 100 Å^2. From this clear dependence of trap lifetime on background gas pressure, we envision measuring dipole-dipole collision cross sections by using polar molecules as background and polarizing them with the E-field of the MET.

We have magnetically confined ground state hydroxyl radicals in a MET that allows for the application of a variable E-field to the trapped polar molecules. Diagonalization of an effective Hamiltonian modelling the energy shift of OH in combined E- and B-fields was necessary for accurate Monte Carlo simulation of the trap dynamics. Future experiments could quantify temperature dependent non-adiabatic transition rates between the different surfaces depicted in Fig. 2(f) akin to Majorana transitions observed in atomic magnetic quadrupole traps. Furthermore, higher densities within the MET will facilitate the study of cold OH-OH collisions in variable electric fields. As rather modest electric fields are expected to modify collision cross sections between polar molecules by as much as 10^3 [17], crossed-beam experiments exploiting the MET described here will benefit from both low center-of-mass collision energies and tunable E-fields in the interaction region.

We acknowledge DOE, NIST, and NSF for support. We thank P. Beckingham, H. Green, and E. Meyer for technical assistance. B. Lev is a NRC postdoctoral fellow.

* Electronic address: sawyerbc@colorado.edu
† Present address: Department of Physics, Yale University, New Haven, CT 06520, USA

[1] J. Doyle et al., Eur. Phys. J. D **31**, 149 (2004).
[2] A. V. Avdeenkov, D. C. E. Bortolotti, and J. L. Bohn, Phys. Rev. A **69**, 012710 (2004).
[3] J. J. Gilijamse et al., Science **313**, 1617 (2006).
[4] E. R. Hudson et al., Phys. Rev. A **76**, 063404 (2006).
[5] B. L. Lev et al., Phys. Rev. A **74**, 061402(R) (2006).
[6] D. DeMille, Phys. Rev. Lett. **88**, 067901 (2002).
[7] A. Micheli, G. Brennen, and P. Zoller, Nature Phys. **2**, 341 (2006).
[8] J. J. Hudson et al., Phys. Rev. Lett. **89**, 023003 (2002).
[9] M. G. Kozlov and D. DeMille, Phys. Rev. Lett. **89**, 133001 (2002).
[10] K. M. Jones et al., Rev. Mod. Phys. **78**, 483 (2006).
[11] J. Sage et al., Phys. Rev. Lett. **94**, 203001 (2005).
[12] H.L. Bethlem, G. Berden, and G. Meijer, Phys. Rev. Lett. **83**, 1558 (1999).
[13] J. Bochinski et al., Phys. Rev. Lett. **91**, 243001 (2003).
[14] J. Weinstein et al., Nature **395**, 148 (1998).
[15] S. Y. T. van de Meerakker et al., Phys. Rev. Lett. **94**, 023004 (2005).
[16] T. Rieger et al., Phys. Rev. Lett. **95**, 173002 (2005).
[17] A. Avdeenkov and J. Bohn, Phys. Rev. A **66**, 052718 (2002).
[18] J. van Veldhoven H. L. Bethlem and G. Meijer, Phys. Rev. Lett. **94**, 083001 (2005).
[19] D. Wang et al., Phys. Rev. Lett. **93**, 243005 (2004).
[20] W. C. Campbell et al., arXiv:physics/0702071 (2007).
[21] T. V. Tscherbul and R. Krems, Phys. Rev. Lett. **97**, 083201 (2006).
[22] C. Ticknor and J. L. Bohn, Phys. Rev. A **71**, 022709 (2005).
[23] M. Lara et al., Phys. Rev. A **75**, 12704 (2007). P. Soldan and J. M. Hutson, Phys. Rev. Lett. **92**, 163202 (2004).
[24] R. V. Krems, Phys. Rev. Lett. **96**, 123202 (2006).
[25] H. J. Lewandowski et al., Chem. Phys. Lett. **395**, 53 (2004).
[26] D. Proch and T. Trickl, Rev. Sci. Instrum. **60**, 713 (1988).
[27] J. Bochinksi et al., Phys. Rev. A **70**, 043410 (2004).
[28] E. R. Hudson et al., Eur. Phys. J. D **31**, 351 (2004).
[29] E. R. Hudson et al., Phys. Rev. Lett. **96**, 143004 (2006).
[30] B. Sawyer et al., (in preparation).